ЖЭТФ, 2014, том 146, вып. 4 (10), стр. 741–746

INFLUENCE OF THE SPATIAL AND TEMPORAL DISTRIBUTION OF AN INCIDENT LASER BEAM PROFILE ON THE ENERGY DISTRIBUTION OF IONIZED PHOTOELECTRONS

V. M. Petrović, T. B. Miladinović*

Department of Physics, Faculty of Science, Kragujevac University
34000, Kragujevac, Serbia

Received May 29, 2014

We discuss the effects of two different spatial and temporal laser beam profiles on the energy distribution of ionized photoelectrons. Two types of profiles of laser radiation, Gaussian and Lorentzian, are considered. The influence of the nonzero initial momentum of ejected photoelectrons is observed. We find that selection of the laser beam profile influences the maximal energy distribution. It is also shown that the nonzero initial electron momentum has a more significant influence for the Lorentzian beam profile.

DOI: 10.7868/S0044451014100083

1. INTRODUCTION

When an intense laser pulse is incident on an atom target, it induces ionization via nonlinear processes. In this paper, the tunnel regime of ionization is analyzed. The theoretical approach to the tunneling problem is based on a single-active-electron approximation, where the idea is that only one electron is involved in the ionization process. Tunneling ionization occurs when the Keldysh parameter $\gamma = \omega\sqrt{2E_i}/F$ [1] is less or much less than unity (here, ω and F are the frequency and the strength of the laser field, and E_i is the ionization potential of the atom or the ion); here and hereafter, we use atomic units ($e = \hbar = m = 1$). The Ammosov–Delone–Krainov (ADK) theory is one of the most widely used theories in this area [2].

Consideration of a spatial–temporal distribution of the laser beam contributes to a better understanding of the aforementioned process. In this paper, the effect of a spatial–temporal profile of the laser beam on the energy distribution is analyzed. In our previous work, we assumed the Gaussian profile of the laser beam for analyzing the energy distribution of ejected electrons taking their initial momentum and the ponderomotive correction into account [3]. Here, we use a modified formula for the Gauss distribution [4] and take one more term from the exponential series. Our numerical calculations show better agreement with the approximation with a larger number of terms. We also analyze the energy distribution of the ejected electron for the Lorenzian beam profile.

*E-mail: tanja.miladinovic@gmail.com

2. THEORY

Gaussian beams are the simplest and often the most desirable type of beam provided by a laser source and allows the highest concentration of light. But although the Gaussian distribution is frequently assumed, there are a few other shapes, such as Lorentzian and flat top, that allow a very uniform distribution of the energy across a given area.

We start with the Gaussian spatial–temporal distribution of the laser field intensity in the form [4]

$$F(\rho,z,t) = \frac{F}{\left[1+(z/z_0)^2\right]^2} \times \exp\left[-\frac{2(\rho/R)^2}{1+(z/z_0)^2} - 2\left(\frac{t}{\tau}\right)^2\right], \quad (1)$$

where z is the coordinate along the light ray, ρ is the axial coordinate that is normal to the light ray, R is the radius of the laser beam, $z_0 = \pi R^2/\lambda$, λ is the laser wave length, t is the emerging time of the ejected electron, τ is the laser pulse duration, and F is the amplitude of the laser field strength.

The Gaussian beam equation given by Eq. (1) assumes that the beam comes to its narrowest width

(called the beam waist) at $z = 0$ [5]. Based on these presumptions, we simplify Eq. (1) to

$$F(\rho, z, t) = F \exp\left[-2\left(\frac{\rho}{R}\right)^2 - 2\left(\frac{t}{\tau}\right)^2\right]. \quad (2)$$

This equation can be written with the spatial dependence part expressed in a more general form,

$$F(\rho, z, t) = F \exp\left[-2\left(\frac{\rho}{R}\right)^n - 2\left(\frac{t}{\tau}\right)^2\right].$$

This modification contains a dimensionless exponent n. It is obvious that the Gaussian is the special case $n = 2$, whereas for larger n, the laser beam profile resembles the flat-top shape [6].

We use the expression for the ionization rate in the framework of the ADK theory [2]. Taking the Gaussian distribution of the laser beam in Eq. (2) into account, we obtain the formula

$$W_{ADK}^{pG2} = W_{ADK} \exp\left(-\frac{\gamma^3 p^2}{3\omega}\right) \times \times \exp\left[-\frac{4}{3}\frac{(2E_i)^{3/2}}{F}\left(\frac{\rho^2}{R^2} + \frac{t^2}{\tau^2}\right)\right], \quad (3)$$

where

$$p = \frac{1}{2}\left(\sqrt{F\eta - 1} + \frac{1}{\eta\sqrt{F\eta - 1}}\right),$$

p is the initial momentum of an ejected electron [7], η is a parabolic coordinate, and in the case where the electron is outside the barrier, $\eta > 1/F$ [8]. Equation (3) corresponds to the second-term expansion of a part of the exponential in Eq. (2).

Usually, the ionization process is saturated, which means that photoelectrons occur inside some definite volume in the laser beam focusing region. In the saturated region, the following condition is satisfied [9]:

$$\int_{-\infty}^{\infty} W\, dt \gg 1. \quad (4)$$

The total number of ions produced during the laser pulse grows very rapidly at a certain value of r (in what follows, ρ), which can be determined to a high degree of accuracy from the condition given by Eq. (4):

$$\int_{-\infty}^{\infty} W\, dt = 1. \quad (5)$$

After substituting Eq. (3) into Eq. (5), we obtain ρ, the radius of the region where saturation of the ionization probability occurs:

$$\rho_{G2}^2 = \frac{3FR^2}{4(2E_i)^{3/2}} \times \times \left[\ln W_{ADK}\sqrt{\frac{3\pi F\tau^2}{4(2E_i)^{3/2}}} - \frac{\gamma^3 p^2}{3\omega}\right]. \quad (6)$$

Inside the region defined by ρ, all atoms are ionized, while outside it, none is ionized.

But as we already noted, the accuracy of the approximation increases if we take more terms from the series of the exponential in Eq. (2) into account. For the third term of the expansion, we obtain

$$W_{ADK}^{pG3} = W_{ADK} \exp\left(-\frac{\gamma^3 p^2}{3\omega}\right) \times \times \exp\left\{-\frac{4(2E_i)^{3/2}}{3F}\left[\frac{\rho^2}{R^2} + \frac{t^2}{\tau^2} + \left(\frac{\rho^2}{R^2} + \frac{t^2}{\tau^2}\right)^2\right]\right\}. \quad (7)$$

Using the above-mentioned procedure and the integral

$$\int_{-\infty}^{\infty} \exp\left\{-a\left[(x^2 + b) + b(b + 2x^2)\right]\right\} dx = = \frac{\exp\left[-ab(1 + b)\right]\sqrt{\pi}}{\sqrt{a + 2ab}},$$

where

$$a = \frac{4(2E_i)^{3/2}}{3F}, \quad b = \frac{\rho^2}{R^2},$$

we obtain from Eq. (7) that

$$\rho_{G3}^2 = \frac{R^2}{4(2(2E_i)^{3/2}/3F - 1)} \times \times \left[\ln W_{ADK}^2\left(\frac{3\pi F}{4(2E_i)^{3/2}}\right) - \frac{2\gamma^3 p^2}{3\omega}\right]. \quad (8)$$

With the condition $t \sim \tau\sqrt{3F/(2E_i)^{3/2}} \ll \tau$ and according to Refs. [3, 10], the final energy of the ejected electron is

$$E_{max} = \frac{p^2}{2} + \frac{F^2}{4\omega^2}\exp\left(-\frac{\rho^2}{R^2}\right). \quad (9)$$

For a Gaussian laser beam, substituting ρ_{G2}^2 and ρ_{G3}^2 in Eq. (9) yields

$$E_{max}^{G2} = \frac{p^2}{2} + \frac{F^2}{4\omega^2}\exp\left\{-\frac{1}{R^2}\frac{3FR^2}{4(2E_i)^{3/2}} \times \times \left[\ln W_{ADK}\sqrt{\frac{3\pi F\tau^2}{4(2E_i)^{3/2}}} - \frac{\gamma^3 p^2}{3\omega}\right]\right\}, \quad (10)$$

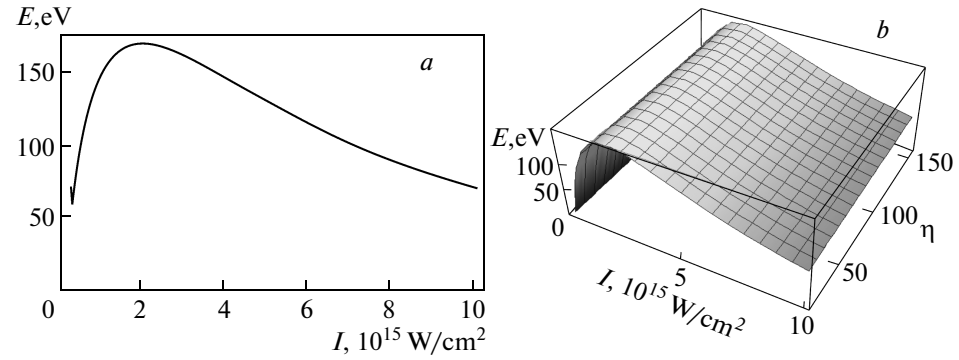

Fig. 1. Dependence of the energy distribution E^{G2}_{max} on the field intensity $I = 10^{14}$–10^{16} W/cm^2 for a nonzero initial momentum is shown as (a) a 2D graph for the fixed parabolic coordinate $\eta = 150$ and (b) a 3D graph for the parabolic coordinate $\eta = 15$–150

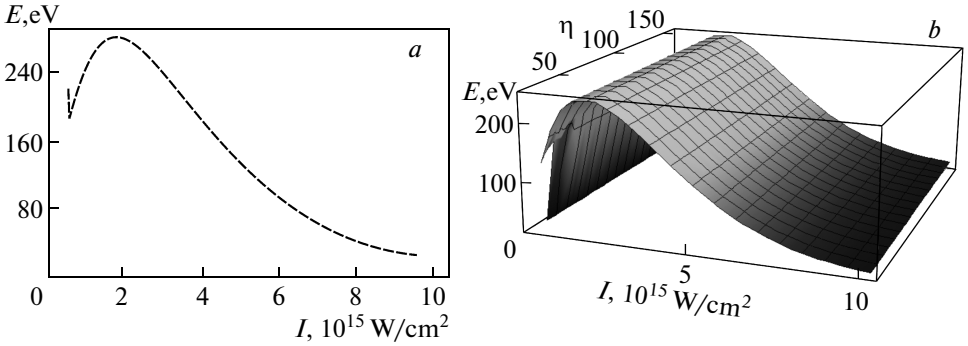

Fig. 2. The same as in Fig. 1 for E^{G3}_{max}

$$E^{G3}_{max} = \frac{p^2}{2} + \frac{F^2}{4\omega^2} \exp\left\{ -\frac{1}{R^2} \frac{R^2}{4[2(2E_i)^{3/2}/3F - 1]} \times \right.$$

$$\left. \times \left[\ln W^2_{ADK} \frac{3\pi F}{4(2E_i)^{3/2}} - \frac{2\gamma^3 p^2}{3\omega} \right] \right\}. \quad (11)$$

We also studied the energy distribution for a Lorentzian laser beam. Just recently, there has been growing interest in the Lorentz beam since it was introduced by Gawhary and Severini [11]. Several temporal profiles for the Lorentzian distribution can be found and some of them include the Gaussian beam as the core of their spatial profile. However, we have chosen the spatial–temporal distribution of the field strength in the form [12, 13]

$$F(\rho, z, t) = \frac{F}{\left[1 + \left(\frac{\rho}{R}\right)^2\right] \left[1 + \frac{4}{1+\sqrt{2}} \left(\frac{t}{\tau}\right)^2\right]}. \quad (12)$$

The corresponding ionization rate is

$$W^{pL2}_{ADK} = W_{ADK} \left(1 + \frac{\rho^2}{R^2} + \frac{t^2}{\tau^2}\right)^{2n^* - 3/2} \times$$

$$\times \exp\left(-\frac{\gamma^3 p^2}{3\omega}\right) \exp\left[-\frac{2(2E_i)^{3/2}}{3F} \left(\frac{t}{\tau} + \frac{\rho}{R}\right)^2\right], \quad (13)$$

where n^* denotes the effective quantum number. By a similar procedure, using the integral

$$\int_{-\infty}^{\infty} \left(1 + \frac{x^2}{3}\right) \exp\left[-b(a+x)^2\right] dx =$$

$$= \frac{\left[1 + 2(3 + a^2)b\right] \sqrt{\pi}}{6},$$

where

$$a = \frac{\rho}{R}, \quad b = \frac{2(2E_i)^{3/2}}{3F},$$

we deduce from Eq. (13) that

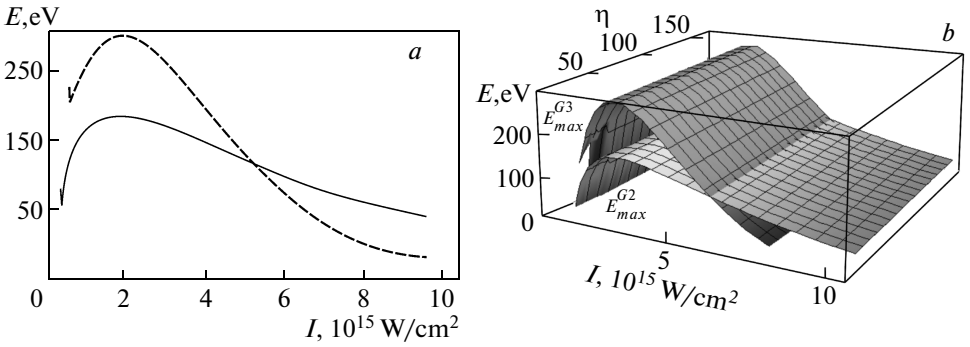

Fig. 3. Comparison of E_{max}^{G2} (solid line) and E_{max}^{G3} (dashed line): (a) a 2D graph and (b) a 3D graph

$$\rho_{L2}^2 = R^2 \left\{ \left[1 + 6 \frac{\exp\left(\dfrac{\gamma^3 p^2}{3\omega}\right) \left[\dfrac{2(2E_i)^{3/2}}{3F}\right]^{3/2}}{\tau W_{ADK}\, \pi^{1/2}} \right] \times \right.$$

$$\left. \times \frac{3F}{4(2E_i)^{3/2}} - 3 \right\}. \quad (14)$$

For the Lorenzian beam shape, the final energy of the ejected photoelectron has the form

$$E_{max} = \frac{p^2}{2} + \frac{F^2}{4\omega^2} \frac{1}{1 + (\rho_{L2}/R)^2}, \quad (15)$$

$$E_{max}^{L2} = \frac{p^2}{2} + \frac{F^2}{4\omega^2} \times$$

$$\times \left\{ 1 + \left[\left(1 + 6 \frac{\exp\left(\dfrac{\gamma^3 p^2}{3\omega}\right) \left[\dfrac{2(2E_i)^{3/2}}{3F}\right]^{3/2}}{\tau W_{ADK}\, \pi^{1/2}} \right) \times \right.\right.$$

$$\left.\left. \times \frac{3F}{4(2E_i)^{3/2}} - 3 \right] \right\}^{-1}. \quad (16)$$

We used only the second-term approximation for this beam shape because the calculation is too complicated for more terms.

3. ANALYSIS

We analyzed the effects of spatial–temporal laser beam profiles on the energy distribution of the ejected photoelectrons for the tunnel ionization process with $\gamma = 0.3$. We chose the pulse profiles to be Gaussian and Lorentzian. The laser beam is a linearly polarized monochromatic plane wave incident along the z direction. We observed a single ionized atom of argon exposed to the CO_2 laser field. The first ionization energy is $E_i = 15.96$ eV, i. e., $E_i = 0.5791$ a. u.

The theoretical energy spectrum of the ejected photoelectrons was obtained from Eq. (9) under the assumption that all the electrons were accelerated by the ponderomotive potential in the focal plane and the initial kinetic energy was nonzero. Figure 1 shows the energy distribution of these electrons for the Gaussian laser beam, based on Eq. (10).

Figure 2 presents the result obtained for the third-degree expansion for a Gaussian beam, based on Eq. (11). To complete the picture of the observed effect, we compare these two expansions and obtain the graphs in Fig. 3. As can be seen from Fig. 3a, the shape becomes narrower for E_{max}^{G3} compared to E_{max}^{G2}. Both graphs first show a rapid energy decrease for some laser field intensity interval; after that, the energy considerably increases up to some maximum value and then decreases for a monotonic increase in the laser field intensity. The E_{max}^{G3} curve decreases much faster than E_{max}^{G2}, especially in the higher-energy region, above $I \approx 4 \cdot 10^{15}$ W/cm^2. As a result, at higher field intensities, the photoelectron energy spectrum for E_{max}^{G2} lies in the energy range much lower than for E_{max}^{G3}. The maximum energy of the ejected photoelectron of an argon atom is higher for E_{max}^{G3} than for E_{max}^{G2}. It is also shifted to the lower field intensity. The laser field intensity at which the maximum energy is achieved for the Gaussian laser profile is $I = 1.91 \cdot 10^{15}$ W/cm^2, $E_{max}^{G2} = 170.868$ eV and $I = 1.83 \cdot 10^{15}$ W/cm^2, $E_{max}^{G3} = 285.911$ eV. In Fig. 3b, this dependence is shown as a function of the parabolic coordinate η, i. e., the nonzero initial momentum.

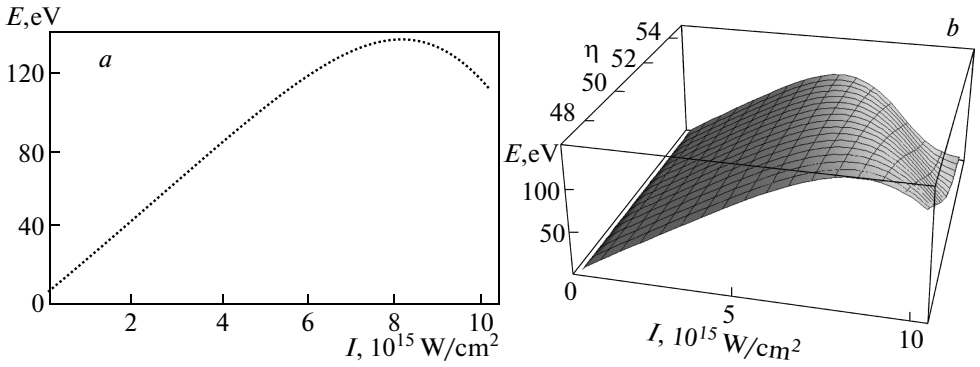

Fig. 4. Dependence of the energy distribution E_{max}^{L2} on the field intensity $I = 10^{14}$–10^{16} W/cm^2 for a nonzero initial momentum shown as (a) a 2D graph for the fixed parabolic coordinate $\eta = 47$, and (b) a 3D graph for the parabolic coordinate $\eta = 45$–55

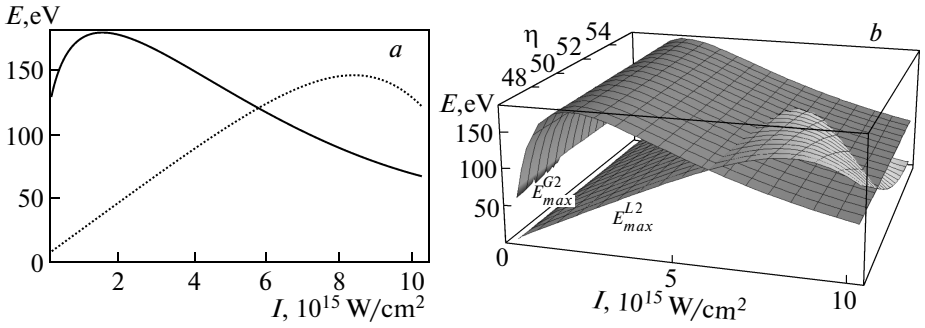

Fig. 5. Comparison of the energy distribution for E_{max}^{G2} and E_{max}^{L2} at the field intensity $I = 10^{14}$–10^{16} W/cm^2 shown as (a) a 2D graph for the fixed parabolic coordinate $\eta = 47$, with the solid line representing E_{max}^{G2} and the dotted line, E_{max}^{L3}, and (b) a 3D graph for the parabolic coordinate $\eta = 45$–55

Next, we analyzed the aforementioned distribution for the Lorentzian beam. According to Eq. (16), the 2D and 3D graphs shown in Fig. 4 are obtained for E_{max}^{L2}.

The characteristic of the maximum energy distribution for a Lorentzian laser beam, E_{max}^{L2}, can be presented in comparison with the Gaussian E_{max}^{G2} assuming the same laser field intensities and values of the parabolic coordinate. Both graphs are shown in Fig. 5.

According to our observations for Gaussian and Lorentzian laser beam profiles, the energy distribution dependence of the laser field intensity is nonlinear and the amplitude is higher for the Gaussian profile than for the Lorentzian one. It is obvious that the decrease corresponding to E_{max}^{G2} is more significant than the one corresponding to E_{max}^{L2}. In Fig. 5a, we also show that the maximum of the energy distribution for E_{max}^{L2} is shifted to the higher laser field intensities. As we already noted, the laser field intensity at which the energy distribution maximum for the Gaussian laser profile is attained is $I = 1.91 \cdot 10^{15}$ W/cm^2 with $E_{max}^{G2} = 170.868$ eV, while in the case of a Lorentzian profile, it is $I = 8.19 \cdot 10^{15}$ W/cm^2 with $E_{max}^{L2} = 135.417$ eV. From Fig. 5b, we can see that the influence of the initial momentum of the ejected photoelectrons is more significant for the Lorentzian distribution. As above, the energy E_{max}^{L2} decreases with an increase in the parabolic coordinate η more rapidly.

4. CONCLUSION

We considered the energy distribution of the ejected photoelectron for the tunnel ionization process in the framework of the ADK theory. The range of laser intensities $I = 10^{14}$–10^{16} W/cm^2 was examined. The main results in this work can be summarized as follows: the considered energy distribution depends on the temporal and spatial distribution of laser beam

profiles, and the nonzero initial electron momentum affects this distribution. All effects depend on the intensity of the applied laser field.

This work was supported in part by the Serbian Ministry of Education, Science, and Technological Development, Republic of Serbia through the projects 171021 and 171020.

REFERENCES

1. L. V. Keldysh, Zh. Eksp. Teor. Fiz. **48**, 1692 (1965).
2. V. M. Ammosov, N. B. Delone, and V. P. Krainov, Zh. Eksp. Teor. Fiz. **91**, 2008 (1986).
3. T. B. Miladinović, J. M. Stevanović, M. M. Radulović, and V. M. Ristić, Phys. Scripta **T149**, 014047 (2012).
4. I. I. Bondar, V. V. Suran, and D. I. Bondar, Phys. Rev. A **88**, 023407 (2013).
5. V. N. Tokarev, J. Lopez, S. Lazare, and F. Weisbuch, Appl. Phys. A **76**, 385 (2003).
6. C. G. Gómez, Master Thesis, *Laser Beam Shaping*, Brno University of Technology, Brno (2012); http://repositorio. unican. es/xmlui/bitstream/handle/10902/1483/349738.pdf?sequence=1.
7. D. Bauer, *Theory of Intense Laser–Matter Interaction*, Max-Planck Institute, Heidelberg, Germany (2006).
8. L. D. Landau and E. M. Lifshitz, *Quantum Mechanics*: *Non-Relativistic Theory*, Pergamon Press, Oxford (1991), p. 295.
9. V. P. Krainov and Z. S. Mulyukov, Laser Phys. **4**, 509 (1994).
10. V. P. Krainov and V. M. Ristić, Zh. Eksp. Teor. Fiz. **101**, 1479 (1992).
11. O. E. Gawhary and S. Severini, J. Opt. A **8**, 409 (2006).
12. S. L. David and H. A. John, in *Proc. SPIE* (*Laser Beam Shaping VI*) **5876** (2005).
13. http://www.diss.fuberlin.de/diss/servlets/MCRFile NodeServlet /FUDISS_derivate_000000005776/09_Chapter05.pdf.